ACS APPLIED MATERIALS & INTERFACES

Research Article

www.acsami.org

# Fabrication of a Visible-Light-Driven Plasmonic Photocatalyst of $AgVO_3$@AgBr@Ag Nanobelt Heterostructures

Yan Sang, Long Kuai, Changyu Chen, Zhen Fang, and Baoyou Geng*

Center for Nano Science and Technology, College of Chemistry and Materials Science, Key Laboratory of Functional Molecular Solids, Ministry of Education, Anhui Laboratory of Molecular-Based Materials, Anhui Normal University, Wuhu 241000, P. R. China

**ABSTRACT:** In this article, $AgVO_3$@AgBr@Ag nanobelt heterostructures were fabricated as an efficient visible-light photocatalyst through a hydrothermal process, an anion-exchange reaction, and a light-induced reduction. SEM and TEM characterization revealed that anion exchange followed by light-induced reduction is an efficient method to synthesize well-dispersed AgBr@Ag nanoparticles on the surface of $AgVO_3$ nanobelts. The composite photocatalyst efficiently combines visible-light active AgBr and $AgVO_3$ with the surface plasmon resonance (SPR) effect of Ag nanoparticles. The obtained catalyst displayed a high performance for removing organic dye in the range of visible light. This improved visible-light response likely originates from a synergistic effect of the different components. This work provides a versatile approach for accessing efficient, stable, and recyclable visible-light-driven plasmonic photocatalysts.

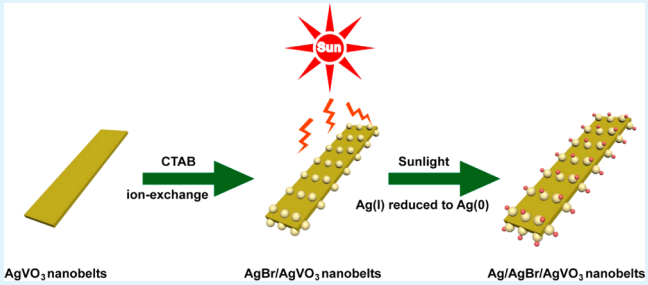


**KEYWORDS:** *$AgVO_3$@AgBr@Ag, heterostructures, plasmonic photocatalyst, ion exchange, visible-light induction, catalysis*

## 1. INTRODUCTION

Recently, visible-light-induced plasmonic photocatalysts have attracted tremendous attention because of their ability to utilize solar energy in the visible−infrared range, resulting in their great potential for use in solving current environment and energy problems.[1−4] In particular, noble-metal−semiconductor nanocomposites have been of significant research interest as an important type of visible-light-induced plasmonic photocatalyst because they possesses the combined merits of different materials.[5] For one merit, some noble metals (Au or Ag) possess a surface plasmon resonance (SPR) effect that can greatly enhance the width of the absorption bands, especially those leading to the visible-light region.[6] For another merit, some semiconductor nanocomposites have been recognized as efficient visible-light photocatalysts because of their exceptional response to visible light.[7,8] In addition, synergism between the support material and the noble metal can make the catalyst more stable and can enhance its photocatalytic performance under visible-light irradiation.[5] Currently, much research on Ag/AgX (X = Br or Cl) has been performed, and the results have revealed that these structures possess excellent performance for the removal of poisonous chemicals under visible-light illumination.[9−13] However, the silver halide species (AgX, X = Br or Cl) always suffers from decomposition under sunlight irradiation, resulting in its poor involvement in the photocatalytic reaction and thus reducing the stability and efficiency of the catalyst. Additionally, silver nanoparticles produced by silver halide are mostly large and disordered, which adversely impacts their SPR effect that relies on the shape, size, and distribution of the noble metal.[14−18]

Herein and with regard to all of the problems mentioned earlier, we purposed to design a three-component system in which the newly added material will improve the general plasmonic photocatalytic performance as well as serve as a support on which the Ag/AgX (X = Br or Cl) will be homogeneously dispersed. In this case, we chose a silver vanadate ($AgVO_3$) nanobelt as the support material because it is not only an efficient visible-light-driven photocatalyst but also has a large surface area, making it a perfect candidate.[19−21] Therefore, our goal was to develop an efficient approach to obtain a $AgVO_3$@AgBr@Ag composite photocatalyst that has both high activity and stability. Figure 1 illustrates the synthetic procedure for the $AgVO_3$@AgBr@Ag hybrid.

First, $AgVO_3$ nanobelts were obtained by a hydrothermal process using $AgNO_3$ and $NH_4VO_3$ as precursors. The as-obtained $AgVO_3$ nanobelts exhibit a relatively high photochemical stability under visible-light irradiation that is more stable than silver halide. Second, through an ion-exchange reaction, AgBr NPs were easily deposited on the surface of the $AgVO_3$ nanobelts by a reaction between $AgVO_3$ nanobelt crystals and hexadecyltrimethylammonium bromide (CTAB) aqueous solutions at room temperature. Then, the as-obtained AgBr particles were partially reduced under sunlight irradiation. Lastly, AgBr@Ag particles were loaded on the surface of $AgVO_3$ nanobelts. The $AgVO_3$@AgBr@Ag hybrid nanocomposites were successfully fabricated, and, as expected, they display

Received: January 10, 2014
Accepted: March 13, 2014
Published: March 13, 2014

   dx.doi.org/10.1021/am5002019 | ACS Appl. Mater. Interfaces 2014, 6, 5061−5068

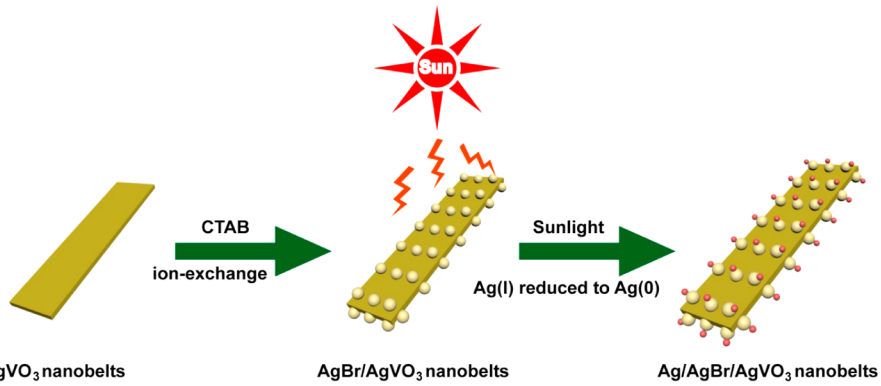


**Figure 1.** Schematic of the synthetic route to the $AgVO_3$@AgBr@Ag nanobelt heterostructures.

superior photocatalytic performance, possessing high visible-light activity (AgBr, $AgVO_3$) and good electron conductivity (Ag).

## 2. EXPERIMENTAL SECTION

**2.1. Chemicals.** $NH_4VO_3$, CTAB (Sinopharm Chemical Reagent Co., Ltd.), and $AgNO_3$ (Shanghai Shenbo Chemical Co., Ltd.) were analytic grade and used without further purification.

**2.2. Synthesis of the $AgVO_3$ Nanobelt.** The $AgVO_3$ nanobelt crystals were synthesized through a hydrothermal process. Typically, 0.0517 g of $AgNO_3$ and 0.0351 g of $NH_4VO_3$ were each dissolved in 10 mL of distilled water. The obtained aqueous solutions were mixed together and stirred for 30 min at room temperature. Then, the mixed solution was transferred into a 30 mL Teflon-lined stainless steel autoclave, which was heated at 180 °C and maintained for 12 h in an oven. Lastly, the product was collected after filtering, washing with water/ethanol, and drying in a vacuum oven (60 °C, 12 h).

**2.3. Synthesis of Belt-Like $AgVO_3$@AgBr@Ag Heterostructures.** The $AgVO_3$@AgBr@Ag hybrids were fabricated through ion exchange between $AgVO_3$ nanobelts and CTAB in distilled water. CTAB was the source of $Br^-$, which could be readily replaced by $VO_3^-$ in the $AgVO_3$ nanobelt crystals to form AgBr. AgBr is easily reduced to Ag under sunlight. The belt-like $AgVO_3$ crystals were used both as the support and the silver ion source. Briefly, 1 mmol of the obtained $AgVO_3$ nanobelt crystals and 1 mmol of CTAB were each dissolved in 20 mL of deionized water with constant stirring. Under stirring, these solutions were mixed together and maintained for 60 min. After that, the solution was irradiated by sunlight for about 4 h until the yellow precipitate turned gray. The final precipitate was dried (60 °C, 12 h) and gathered for subsequent use. In this case, different molar ratios of CTAB to $AgVO_3$ (1:1, 1:2, 1:4, and 1:8) were selected for comparison.

**2.4. Characterization.** The morphology and structure of the as-prepared products were characterized by scanning electron microscopy (SEM, Hitachi S-4800), transmission electron microscopy (TEM) and HRTEM (TEM, Tecnai G2 20S-TWIN, Holland). The phase purity and components of the products were confirmed by X-ray diffraction (XRD, Philips X'Pert with Cu $K\alpha_1$ radiation ($\lambda$ = 1.54060 Å)) and X-ray photoelectron spectroscopy (XPS, ESCALAB 250 with monochromatized Mg $K\alpha$ irradiation as the source).

**2.5. Photocatalytic Reactions.** Rhodamine B (RhB) was selected as a model pollutant to evaluate the catalytic performance of the obtained heterostructures. To achieve effective contrast, the dosage of the catalysts in each experiment was kept at 0.2 g, and the volume RhB was 60 mL (10 mg/L). The catalytic experiments were performed at room temperature and were irradiated with a 300 W Xe arc lamp ($\lambda \geq 420$ nm). UV−vis absorption spectroscopy (UV-2450, Shimadzu) was used to record the reaction process.

**2.6. Detection of Hydroxyl Radicals ($OH^•$).** Typically, 0.1 g of the as-prepared product was suspended in a terephthalic acid (TA) aqueous solution (20 mL, $5 \times 10^{-4}$ M), and the pH was adjusted using concentrated NaOH ($2 \times 10^{-3}$ M). The solution was stirred for 15 min to reach homogeneity at room temperature. After that, the solution was irradiated with a 300 W Xe lamp. About 3 mL of the solution was removed at 15 min intervals and was separated by centrifugation at 9500 rpm to remove the photocatalyst. The fluorescence intensity at 426 nm was monitored on a Hitachi F-4500 fluorescence spectrophotometer excited by 315 nm light.

## 3. RESULTS AND DISCUSSION

**3.1. Morphology and Crystal Structure of $AgVO_3$.** Figure 2a shows a low-magnification SEM image of the products, which clearly reveals that the as-obtained product consists of ultralong nanobelts with a length of several tens of micrometers. Figure 2b further confirms that the products are nanobelts with a width of about 150−200 nm, which is consistent with the TEM result (Figure 2c). Additionally, the XRD (Figure 2d) pattern matches well with the monoclinic $\beta$-$AgVO_3$ (JCPDS 29-1154) calculated lattice constants of $a$ = 17.87 Å, $b$ = 3.580 Å, and $c$ = 8.036 Å.

**3.2. Characterization of the $AgVO_3$@AgBr@Ag Photocatalyst.** The XRD pattern of the product (Figure 3) shows that $Ag^0$, AgBr, and $\beta$-$AgVO_3$ are coexistent. The intensity of the $Ag^0$ peaks covered by the background is very weak. The existence of $Ag^0$ is further demonstrated in the XPS spectrum (as shown in Figure 6d).

Through ion exchange, the surface of the $\beta$-$AgVO_3$ nanobelts could be decorated by AgBr particles (Figure 4). Figure 4a reveals that the morphology of the products is unchanged after the ion-exchange process. An enlarged SEM image (Figure 4b) shows that some small irregular particles appear on the surface of the $AgVO_3$ nanobelts. The TEM image in Figure 4c also demonstrates that many nanoparticles are uniformly anchored on the nanobelts. The HRTEM image of a single nanoparticle (Figure 4d) clearly reveals that the lattice spacing of the particle is 0.236 nm, which can be indexed to the (111) spacing of Ag (JCPDS 03-0921). It is noteworthy from the HRTEM image that all of the Ag dots have a ring-like structure around them, which is probably damaged AgBr caused by the high-energy electron beam. We also found that the size and distribution of the nanoparticles are largely dependent on the molar ratio of $AgVO_3$ to CTAB.

SEM images of the $AgVO_3$@AgBr@Ag nanobelts with different molar ratios of $AgVO_3$ to CTAB are shown in Figure 5. All of them inherited the morphology of the original belt-like $AgVO_3$ crystals. The surface of the $AgVO_3$ crystals is covered in situ by AgBr@Ag nanodots. Careful observation revealed that the abundance of small spots differs with the ratio of CTAB. The lower the ratio of CTAB/$AgVO_3$ (e.g., 1:4, Figure 5a), the smaller the nanospots on the nanobelts (e.g., 1:1, Figure 5d). That is, with an increase in the CTAB ratio, the size of the


dx.doi.org/10.1021/am5002019 | ACS Appl. Mater. Interfaces 2014, 6, 5061−5068

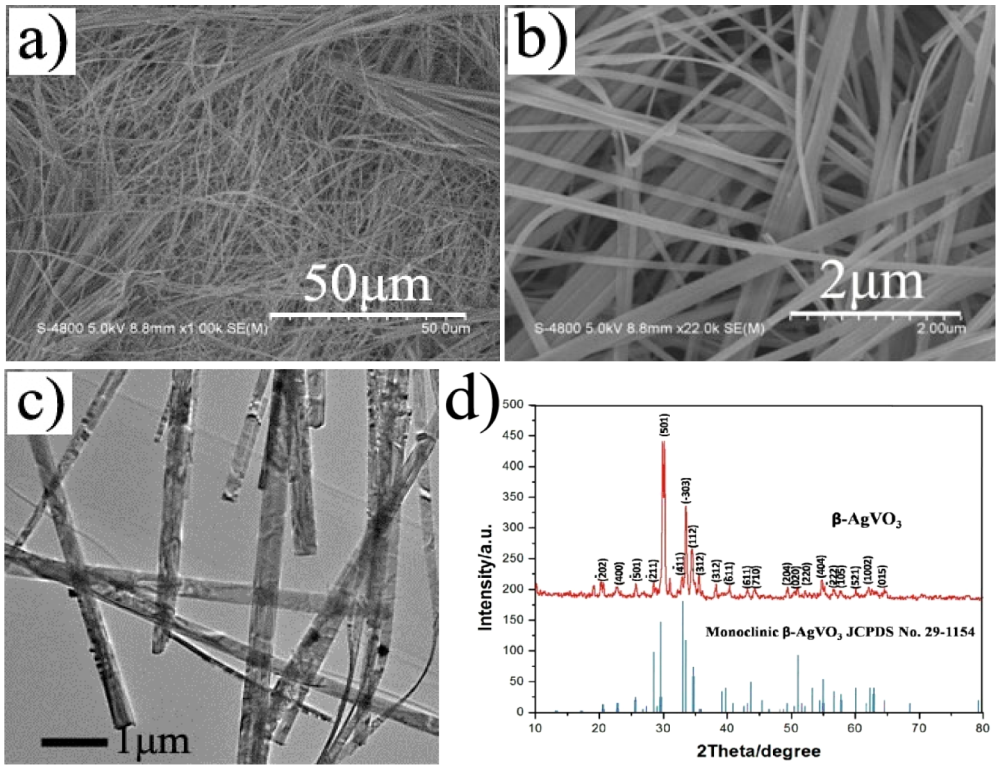


**Figure 2.** (a) Low- and (b) high-magnification SEM and (c) TEM images of the as-prepared $\beta$-$AgVO_3$ nanobelts. (d) XRD pattern of the products.

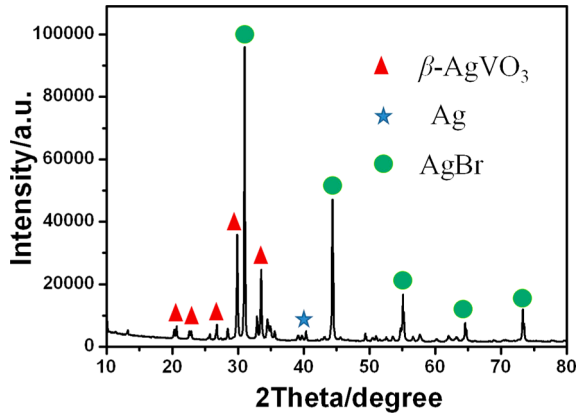


**Figure 3.** XRD pattern of $AgVO_3$@AgBr@Ag obtained by an ion-exchange method.

nanospots on the nanobelts increases, and the surface of the belts becomes coarser, as shown in Figure 5c,d.

The successful decoration of $\beta$-$AgVO_3$ nanobelts with AgBr@Ag nanoparticles was further confirmed by XPS. Figure 6a shows the entire XPS spectrum of the products in which the peaks of Ag, Br, V, and O are found. The C 1s peaks should originate from CTAB. The 516, 524, and 529 eV peaks in Figure 6b can be assigned to V ($2p_{3/2}$), V ($2p_{1/2}$), and O (1s), respectively. The Br 3d peak (Figure 6c) is divided into two peaks at 69.8 and 68.9 eV and should originate from AgBr.[22] The Ag 3d peak is also divided into Ag $3d_{5/2}$ and $3d_{3/2}$ peaks. Specifically, the 367.6 and 373.7 eV peaks originate from $Ag^+$ in AgBr and the 368.1 and 374.1 eV peaks are $Ag^0$ species (Figure 6d, inset).

Figure 7 shows UV−vis diffuse reflectance spectra of the $AgVO_3$, $AgVO_3$@AgBr, and $AgVO_3$@AgBr@Ag nanobelt heterostructures. Clearly, the pure $AgVO_3$ nanobelts mainly absorb energy under 580 nm. After loading with AgBr, the absorption band edge shows an obvious shift to the visible-light region, which is thought to occur from a synergistic effect between AgBr and $AgVO_3$. The enhanced absorption in the visible-light region of $AgVO_3$@AgBr@Ag should be attributed to the SPR effect and electron-transfer efficiency of Ag nanoparticles[10,23] as well as to the visible-light-active component, AgBr.

**3.3. Photodegradation of RhB Dye.** To evaluate the photocatalytic performance of the nanobelt heterostructures, we performed comparative experiments on the photocatalytic degradation of RhB using $AgVO_3$@AgBr@Ag and pure $AgVO_3$ nanobelts as photocatalysts. $C/C_0$ is defined as the degradation efficiency, where $C$ and $C_0$ are the remnant and initial concentration of RhB, respectively. Figure 8a shows the degradation curves of RhB on $AgVO_3$@AgBr@Ag nanobelt heterostructures. It can be clearly seen that RhB is decomposed by about 50% within 2 min in the solution of $AgVO_3$@AgBr@Ag nanobelt heterostructures with $M_{CTAB}/M_{AgVO3}$ = 1:1 and is almost completely decomposed after 12 min. The comparison experiments between $AgVO_3$ nanobelts and different $AgVO_3$@AgBr@Ag nanobelt heterostructures are shown in Figure 8b. Obviously, the single visible-light-active component of the $AgVO_3$ nanobelt photocatalyst will exhibit a lower photocatalytic activity, resulting in a degradation ratio of about 60% in 18 min. However, the degradation rate of $AgVO_3$@AgBr@Ag nanobelt heterostructures ($M_{CTAB}/M_{AgVO3}$ = 1:4) can reach 80% in 18 min. The results also show that the products obtained at a higher ratio of CTAB/$AgVO_3$ have a higher photocatalytic activity under visible-light irradiation.

**3.4. Stability of Photocatalytic Performance.** Recycling experiments were performed to assess the stability of the photocatalyst. Figure 9a shows the experimental results in 14 min. From Figure 9a, it can be seen that the $AgVO_3$@AgBr@Ag


dx.doi.org/10.1021/am5002019 | ACS Appl. Mater. Interfaces 2014, 6, 5061−5068

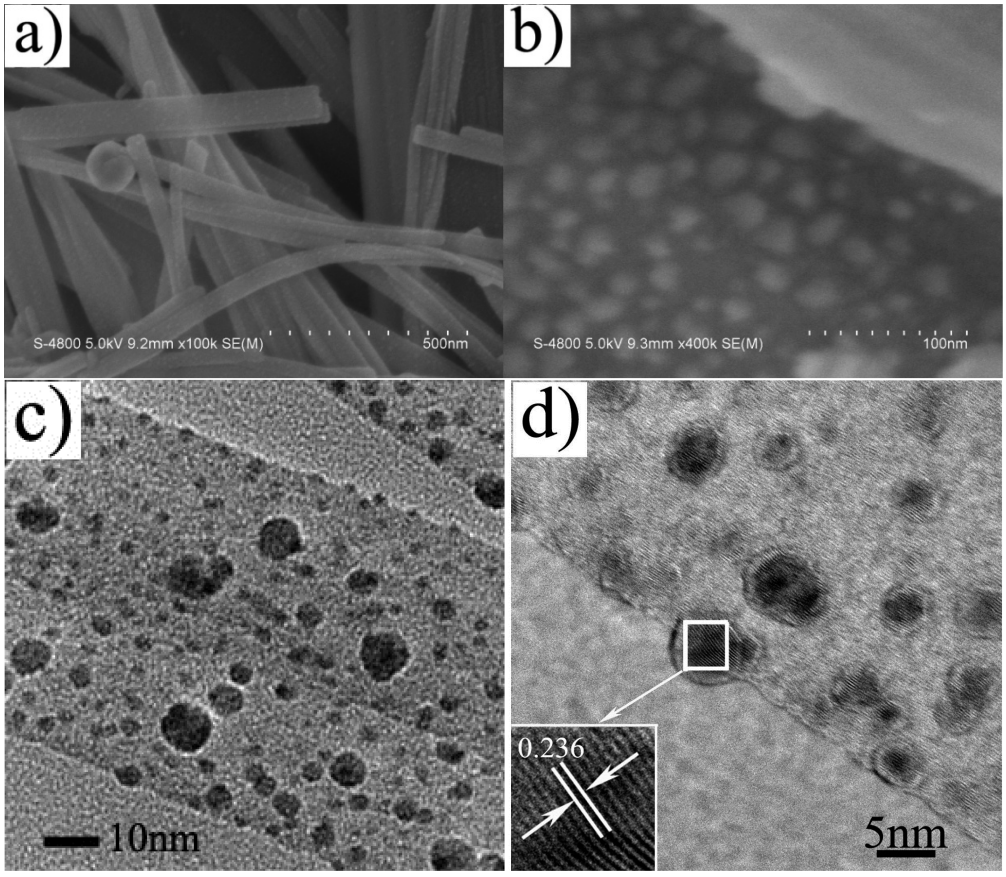


**Figure 4.** (a, b) SEM images of the sample obtained by an ion-exchange method with a 1:4 molar ratio of $AgVO_3$ to CTAB. (c, d) TEM and HRTEM images of the sample.

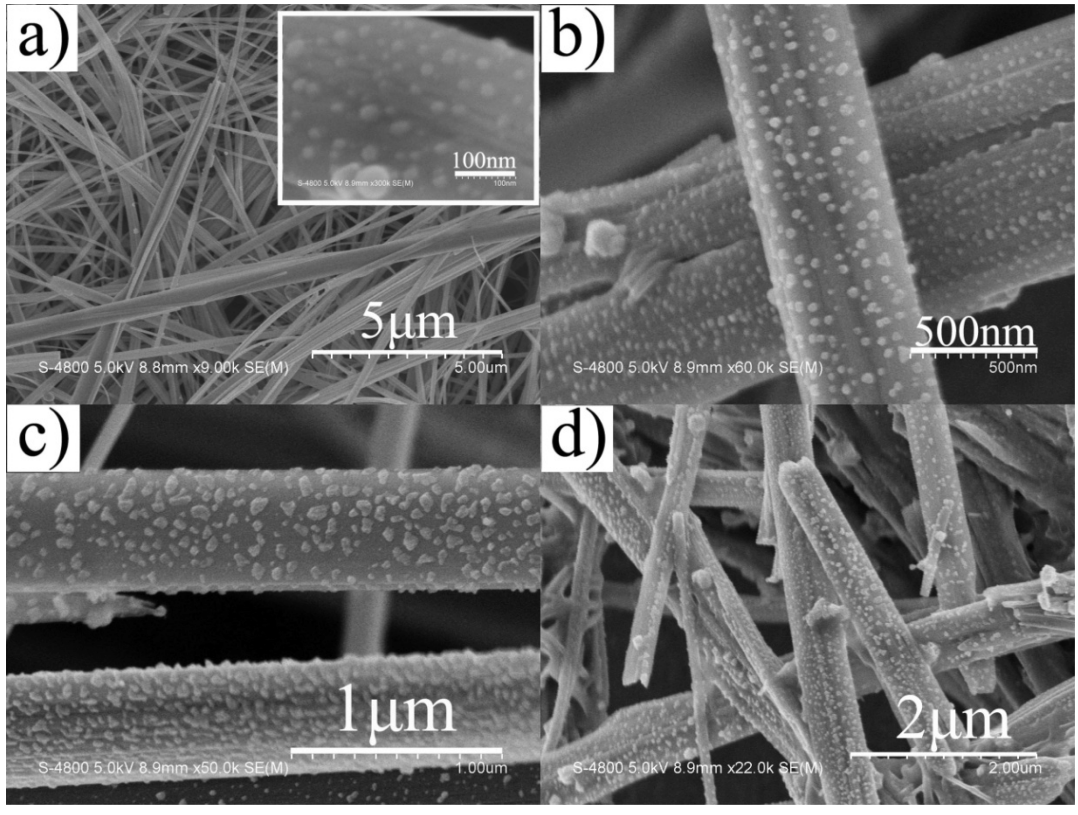


**Figure 5.** SEM images of the products obtained at 180 °C for 10 h with different molar ratios of the precursors ($M_{CTAB}/M_{AgVO3}$): (a) 1:4, (b) 1:2, (c) 3:4, and (d) 1:1.


dx.doi.org/10.1021/am5002019 | ACS Appl. Mater. Interfaces 2014, 6, 5061−5068

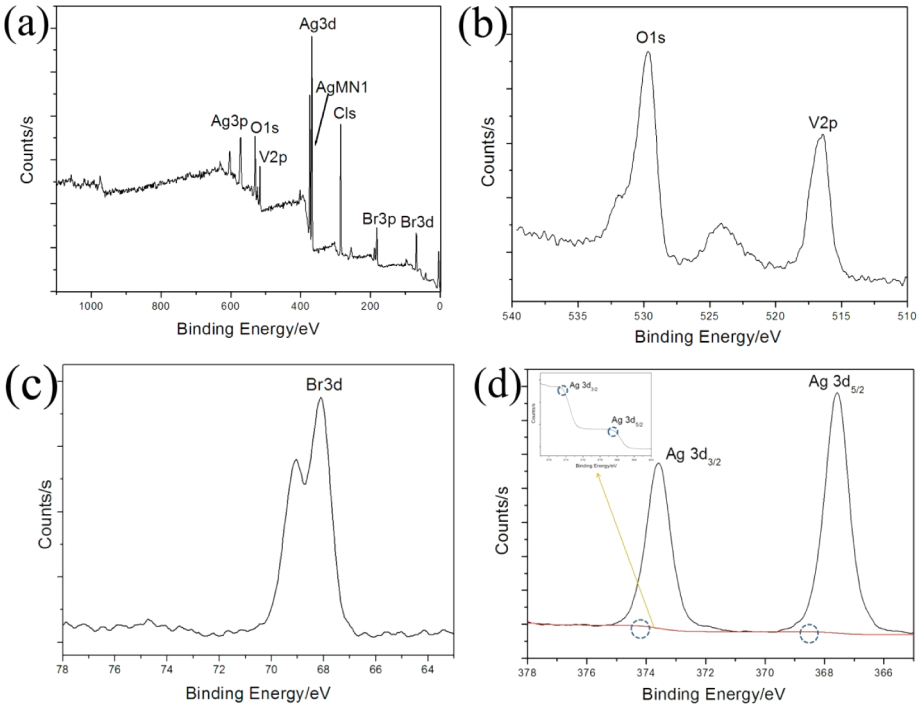


**Figure 6.** XPS spectra of $AgVO_3$@AgBr@Ag ($M_{CTAB}/M_{AgVO3}$ = 1:1): (a) XPS survey spectrum; (b) XPS spectrum of O 1s and V 2p, (c) XPS spectrum of Br3d, (d) XPS spectrum of Ag 3d. The inset is the XPS spectrum of the $Ag^0$ species.

nanobelt heterostructures have a high stability, resulting in a high decomposition ratio even after five cycles. Recycling experiments reveal that the photocatalytic activity shows a slight reduction after the first cycle. The reason for this may be due to some $Ag^+$ ions being transformed into $Ag_2O$, where generated $Ag_2O$ prevents interfacial charge-transfer kinetics between Ag and AgBr. Interestingly, after 56 min of degradation (at the fifth cycle), a slight enhancement can be seen in the photocatalytic activity. This should be attributed to the decomposition of AgBr to Ag under illumination on the surface of the $AgVO_3$ nanobelt. The SPR generated by silver nanoparticles could result in the enhancement of the photocatalytic activity.

The XRD pattern of the $AgVO_3$@AgBr@Ag sample after photocatalysis is shown in Figure 9b, which also reveals the stability of the $AgVO_3$@AgBr@Ag sample. It can be seen that $Ag^0$, AgBr, and $\beta$-$AgVO_3$ still coexist in the sample after photocatalysis. Compared with the $AgVO_3$@AgBr@Ag sample before photocatalysis, the XRD pattern is barely changed after photocatalysis, which also clearly demonstrates that the obtained $AgVO_3$@AgBr@Ag sample has a high stability.

**3.5. Detection and Analysis of Hydroxyl Radicals (OH•).** The existence of hydroxyl radicals (OH•) was characterized as in previous reports.[24,25] Figure 10 shows the photoluminescence (PL) spectra of $AgVO_3$ and $AgVO_3$@AgBr@Ag ($M_{CTAB}/M_{AgVO3}$ = 1:1) in TA solution. As can be seen, the fluorescence intensities at 426 nm of the $AgVO_3$@AgBr@Ag and $AgVO_3$ solution are quite large, but the former is obviously stronger than the latter at the same interval. This implies that the OH• radicals in the $AgVO_3$@AgBr@Ag solution are more easily produced than those in the $AgVO_3$ solution. It should also be noted that there is almost no fluorescence signal without the presence of the photocatalysts.

**3.6. Discussion of a Possible Photocatalytic Mechanism.** Plasmonic enhancements and facile charge transfer resulting from the assistance of metallic Ag are proposed to explain the high photocatalytic activity of the $AgVO_3$@AgBr@Ag nanostructures. Previous research has demonstrated that the SPR effect of Ag nanoparticles plays a very important role in producing high visible-light photocatalytic activity for the oscillation of surface electrons.[26−28] Additionally, the rich conduction band (CB) electrons of noble metals can enhance the reducibility of hybrids, resulting in a decreased recombination opportunity of $e^-$–$h^+$.[29] In particular, the excellent conductivity of Ag nanoparticles greatly promotes interfacial charge-transfer kinetics among Ag, AgBr, and $AgVO_3$. The proposed charge-transfer mechanism for the $AgVO_3$@AgBr@Ag nanobelt heterostructures is illustrated in Scheme 1.

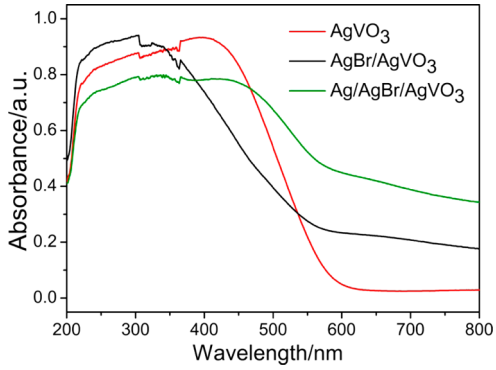


**Figure 7.** UV−vis diffuse reflectance spectra of $AgVO_3$ nanobelts and $AgVO_3$@AgBr@Ag nanobelt heterostructures with a 1:1 molar ratio of CTAB/$AgVO_3$.

AgBr (2.6 eV) and $AgVO_3$ (2.3 eV) are matched in their band gap. The energy of visible light is sufficient to excite the valence band (VB) electrons of $AgVO_3$ and AgBr so that they jump into the conduction band (CB). Because silver is one of the best conductive metals, light-induced electrons can be quickly transferred at the interface of the heterostructures, thus


dx.doi.org/10.1021/am5002019 | ACS Appl. Mater. Interfaces 2014, 6, 5061−5068

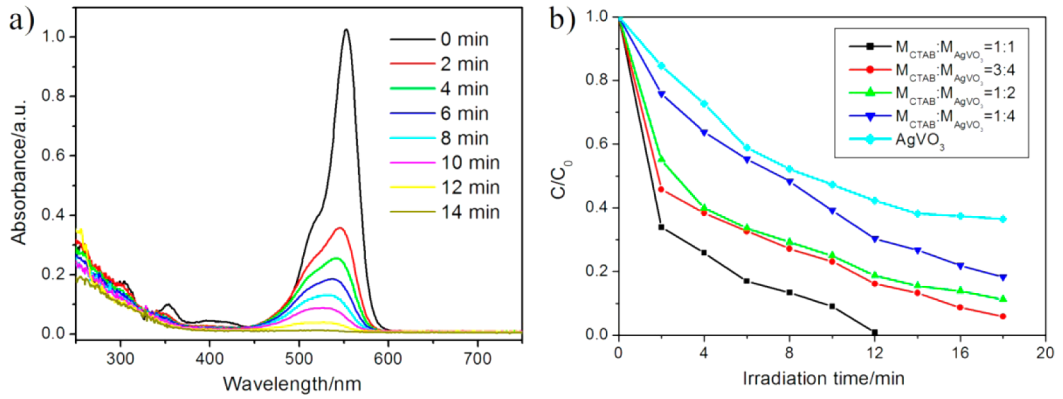


**Figure 8.** (a) Time-dependent degradation curves of RhB with $AgVO_3$@AgBr@Ag ($M_{CTAB}/M_{AgVO3}$ = 1:1) under visible-light irradiation. (b) Time-dependent photodecomposition curves of RhB over different samples ($C_0$ = 10 mg/L, sample = 0.02 g).

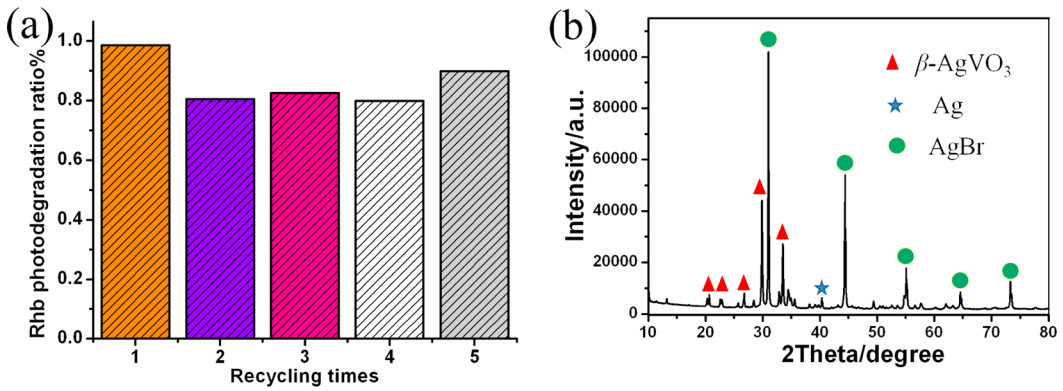


**Figure 9.** (a) Five-cycle recycling experiments of the $AgVO_3$@AgBr@Ag nanobelt heterostructures ($M_{CTAB}/M_{AgVO3}$ = 1:1). (b) XRD pattern of $AgVO_3$@AgBr@Ag after photocatalysis.

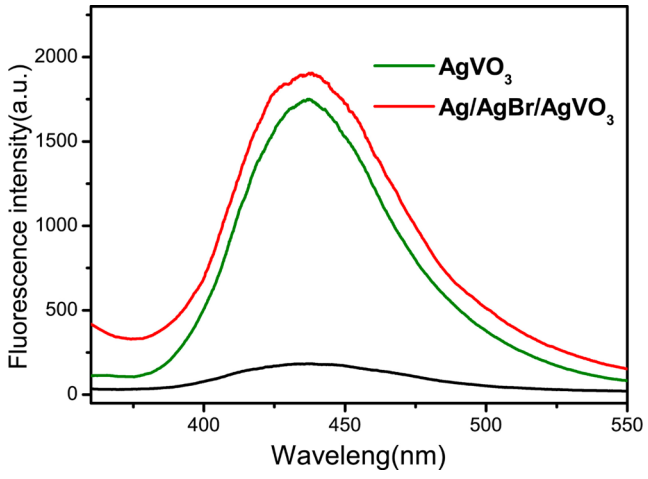


**Figure 10.** $OH^{\bullet}$-trapping PL spectra of $AgVO_3$ and $AgVO_3$@AgBr@Ag ($M_{CTAB}/M_{AgVO3}$ = 1:1) in terephthalic acid solution after irradiation for 15 min.

**Scheme 1. Proposed Mechanism for Photocatalysis of the $AgVO_3$@AgBr@Ag Nanobelt Heterostructures**

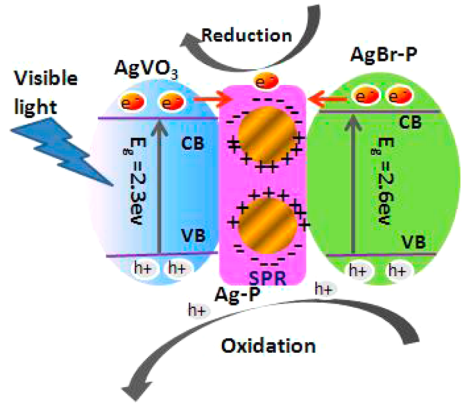


avoiding recombination with the excited holes. Then, these electrons are received by adsorbed RhB molecules, resulting in its reduction, or they are trapped by $O_2$ and $H_2O$ to form $O_2^-$ or other reactive species; thus, the recombination between excited electrons and holes can be effectively curbed.[10,30] The remained holes can be directly oxidized by water to hydroxyl radicals, which plays a very important role in the degradation of an organic molecule.[24] These highly reactive $O_2^{\bullet}$ and $OH^{\bullet}$ species are sufficient to destroy the structure of an organic molecule, leading to the subsequent decomposition of the pollutants. The fluorescence detection in Figure 10 confirmed that many hydroxyl radicals exist in the products, which is favorable for enhancing the photocatalytic performance.[22,31,32] In other words, the heterostructure prevents the recombination of the electron−hole pairs with the assistant of plasmonic Ag, thereby generating more $OH^{\bullet}$ or $O_2^{\bullet}$ radicals and resulting in the improvement of the photocatalytic activity.

## 4. CONCLUSIONS

Highly efficient $AgVO_3$@AgBr@Ag nanobelt heterostructures for use as a visible-light plasmonic photocatalyst were fabricated


dx.doi.org/10.1021/am5002019 | ACS Appl. Mater. Interfaces 2014, 6, 5061−5068

through a designed route that included a hydrothermal process, ion-exchange reaction, and light-induced reduction. The obtained photocatalyst could effectively degrade RhB under visible-light irradiation ($\lambda$ > 420 nm). Moreover, recycling experiments revealed that the photocatalyst exhibits excellent stability. The superior performance of the as-obtained photocatalyst should be attributed to the good visible-light-active components (AgBr, $AgVO_3$) and to the SPR effect of the Ag nanoparticles. These results should prove to be valuable for the synthesis of Ag/different semiconductor catalysts that possess high catalytic activity.

## AUTHOR INFORMATION


### Corresponding Author

*Phone: (86) 553-3937138. Fax: (86) 553-3869302. E-mail: bygeng@mail.ahnu.edu.cn.


### Notes

The authors declare no competing financial interest.

## ACKNOWLEDGMENTS

This work was supported by the NSFC (20971003 and 21271009), the Key Project of the Chinese Ministry of Education (209060), NCET 11-0888, the Doctoral Fund of the Ministry of Education of China (20123424110002), the Fund of Anhui Province for Outstanding Youth (1308085JGD01), the Key Project of the Anhui Education Committee (KJ2012A143), Outstanding Youth of High Schools (2012SQRL030), and the Program for Innovative Research Team at Anhui Normal University.

## REFERENCES


(1) Fujishima, A.; Honda, K. Electrochemical Photolysis of Water at a Semiconductor Electrode. *Nature* **1972**, *238*, 37−38.

(2) Wang, R.; Hashimoto, K.; Fujishima, A.; Chikuni, M.; Kojima, E.; Kitamura, A.; Shimohigoshi, M.; Watanabe, T. Light-Induced Amphiphilic Surfaces. *Nature* **1997**, *388*, 431−432.

(3) Hoffmann, M. R.; Martin, S. T.; Choi, W.; Bahneman, D. W. Environmental Applications of Semiconductor Photocatalysis. *Chem. Rev.* **1995**, *95*, 69−96.

(4) Cheng, H. F.; Huang, B. B.; Wang, P.; Wang, Z. Y.; Lou, Z. Z.; Wang, J. P.; Qin, X. Y.; Zhang, X. Y.; Dai, Y. In Situ Ion Exchange Synthesis of the Novel Ag/AgBr/BiOBr Hybrid with Highly Efficient Decontamination of Pollutants. *Chem. Commun.* **2011**, *47*, 7054−7056.

(5) Tian, Y.; Tatsuma, T. Mechanisms and Applications of Plasmon-Induced Charge Separation at $TiO_2$ Films Loaded with Gold Nanoparticles. *J. Am. Chem. Soc.* **2005**, *127*, 7632−7637.

(6) Awazu, K.; Fujimaki, M.; Rockstuhl, C.; Tominaga, J.; Murakami, H.; Ohki, Y.; Yoshida, N.; Watanabe, T. A Plasmonic Photocatalyst Consisting of Silver Nanoparticles Embedded in Titanium Dioxide. *J. Am. Chem. Soc.* **2008**, *130*, 1676−1680.

(7) Zhang, H. J.; Chen, G. H.; Bahnemann, D. Photoelectrocatalytic Materials for Environmental Applications. *J. Mater. Chem.* **2009**, *19*, 5089−5121.

(8) Zeng, H. B.; Duan, G. T.; Li, Y.; Yang, S. K.; Xu, X. X.; Cai, W. P. Blue Luminescence of ZnO Nanoparticles Based on Non-Equilibrium Processes: Defect Origins and Emission Controls. *Adv. Funct. Mater.* **2010**, *20*, 561−572.

(9) Wang, P.; Huang, B. B.; Qin, X. Y.; Zhang, X. Y.; Dai, Y.; Wei, J. Y.; Whangbo, M. H. Ag@AgCl: A Highly Efficient and Stable Photocatalyst Active under Visible Light. *Angew. Chem., Int. Ed.* **2008**, *47*, 7931−7933.

(10) Kuai, L.; Geng, B. Y.; Chen, X. T.; Zhao, Y. Y.; Luo, Y. C. Facile Subsequently Light-Induced Route to Highly Efficient and Stable Sunlight-Driven Ag-AgBr Plasmonic Photocatalyst. *Langmuir* **2010**, *26*, 18723−18727.

(11) Zhu, M. S.; Chen, P. L.; Liu, M. H. Graphene Oxide Enwrapped Ag/AgX (X=Br, Cl) Nanocomposite as a Highly Efficient Visible-Light Plasmonic Photocatalyst. *ACS Nano* **2010**, *5*, 4529−4536.

(12) An, C. H.; Peng, S.; Sun, Y. G. Facile Synthesis of Sunlight-Driven AgCl:Ag Plasmonic Nanophotocatalyst. *Adv. Mater.* **2010**, *22*, 2570−2574.

(13) Yan, Z. J.; Compagnini, G.; Chrisey, D. B. Generation of AgCl Cubes by Excimer Laser Ablation of Bulk Ag in Aqueous NaCl Solutions. *J. Phys. Chem. C* **2011**, *115*, 5058−5062.

(14) Amendola, V.; Bakr, O. M.; Stellacci, F. A Study of the Surface Plasmon Resonance of Silver Nanoparticles by the Discrete Dipole Approximation Method: Effect of Shape, Size, Structure, and Assembly. *Plasmonics* **2010**, *5*, 85−97.

(15) El-Brolossy, T. A.; Abdallah, T.; Mohamed, M. B.; Abdallah, S.; Easawi, K.; Negm, S.; Talaat, H. Shape and Size Dependence of the Surface Plasmon Resonance of Gold Nanoparticles Studied by Photoacoustic Technique. *Eur. Phys. J.: Spec. Top.* **2008**, *153*, 361−364.

(16) Lu, L. H.; Kobayashi, A.; Tawa, K.; Ozaki, Y. Silver Nanoplates with Special Shapes: Controlled Synthesis and Their Surface Plasmon Resonance and Surface-Enhanced Raman Scattering Properties. *Chem. Mater.* **2006**, *18*, 4894−4901.

(17) Matsubara, K.; Kelly, K. L.; Sakai, N.; Tatsuma, T. Plasmon Resonance-Based Photoelectrochemical Tailoring of Spectrum, Morphology and Orientation of Ag Nanoparticles on $TiO_2$ Single Crystals. *J. Mater. Chem.* **2009**, *19*, 5526−5532.

(18) Tanabe, I.; Matsubara, K.; Standridge, S. D.; Kazuma, E.; Kelly, K. L.; Sakaia, N.; Tatsuma, T. Photocatalytic Growth and Plasmon Resonance-Assisted Photoelectrochemical Toppling of Upright Ag Nanoplates on a Nanoparticulate $TiO_2$ Film. *Chem. Commun.* **2009**, 3621−3623.

(19) Lin, H. S.; Maggard, P. A. Syntheses and Structures of a New Series of Silver-Vanadate Hybrid Solids and Their Optical and Photocatalytic Properties. *Inorg. Chem.* **2008**, *47*, 8044−8052.

(20) Pan, G. T.; Lai, M. H.; Juang, R. C.; Chung, T. W.; Yang, T. K. Preparation of Visible-Light-Driven Silver Vanadates by a Microwave-Assisted Hydrothermal Method for the Photodegradation of Volatile Organic Vapors. *Ind. Eng. Chem. Res.* **2011**, *50*, 2807−2814.

(21) Huang, C. M.; Cheng, K. W.; Pan, G. T.; Chang, W. S.; Yang, T. K. CTAB-Assisted Hydrothermal Synthesis of Silver Vanadates and Their Photocatalytic Characterization. *Chem. Eng. Sci.* **2010**, *65*, 148−152.

(22) Wang, P.; Huang, B. B.; Qin, X. Y.; Zhang, X. Y.; Dai, Y.; Whangbo, M. H. Ag/AgBr/$WO_3{\cdot}H_2O$: Visible-Light Photocatalyst for Bacteria Destruction. *Inorg. Chem.* **2009**, *48*, 10697−10702.

(23) Wang, P.; Huang, B. B.; Zhang, Q. Q.; Zhang, X. Y.; Qin, X. Y.; Dai, Y.; Zhan, J.; Yu, J. X.; Liu, H. X.; Lou, Z. Z. Highly Efficient Visible Light Plasmonic Photocatalyst Ag@Ag(Br, I). *Chem.—Eur. J.* **2010**, *16*, 10042−10047.

(24) Wang, J. X.; Ruan, H.; Li, W. J.; Li, D. Z.; Hu, Y.; Chen, J.; Shao, Y.; Zheng, Y. Highly Efficient Oxidation of Gaseous Benzene on Novel $Ag_3VO_4/TiO_2$ Nanocomposite Photocatalysts under Visible and Simulated Solar Light Irradiation. *J. Phys. Chem. C* **2012**, *116*, 13935−13943.

(25) Yu, J. G.; Wang, W. G.; Cheng, B.; Su, B. L. Enhancement of Photocatalytic Activity of Mesporous $TiO_2$ Powders by Hydrothermal Surface Fluorination Treatment. *J. Phys. Chem. C* **2009**, *113*, 6743−6750.

(26) Zeng, H. B.; Cai, W. P.; Liu, P. S.; Xu, X. X.; Zhou, H. J.; Klingshirn, C.; Kalt, H. ZnO-Based Hollow Nanoparticles by Selective Etching: Elimination and Reconstruction of Metal-Semiconductor Interface, Improvement of Blue Emission and Photocatalysis. *ACS Nano* **2008**, *2*, 1661−1670.

(27) Wang, P.; Huang, B. B.; Zhang, X. Y.; Qin, X. Y.; Jin, H.; Dai, Y.; Wang, Z. Y.; Wei, J. Y.; Zhan, J.; Wang, S. Y.; Wang, J. P.; Whangbo, M. H. Highly Efficient Visible-Light Plasmonic Photocatalyst Ag@AgBr. *Chem.—Eur. J.* **2009**, *15*, 1821−1824.

(28) Hu, C.; Lan, Y. Q.; Qu, J. H.; Hu, X. X.; Wang, A. M. Ag/AgBr/$TiO_2$ Visible Light Photocatalyst for Destruction of Azodyes and Bacteria. *J. Phys. Chem. B* **2006**, *110*, 4066−4072.
(29) Wang, L. J.; Yan, X. W.; Xu, C. L.; Xiao, Z. L.; Yang, L. M.; Zhang, B.; Wang, Q. Q. Photocatalytical Reduction of Disulphide Bonds in Peptides on Ag-Loaded Nano-$TiO_2$ for Subsequent Derivatization and Determination. *Analyst* **2011**, *136*, 3602−3604.
(30) Zhou, X. F.; Hu, C.; Hu, X. X.; Peng, T. W.; Qu, J. H. Plasmon-Assisted Degradation of Toxic Pollutions with Ag-AgBr/$Al_2O_3$ under Visible-Light Irradiation. *J. Phys. Chem. C* **2010**, *114*, 2746−2750.
(31) Yu, J. G.; Dai, G. P.; Huang, B. B. Fabrication and Characterization of Visible-Light-Driven Plasmonic Photocatalyst Ag/AgCl/$TiO_2$ Nanotube Arrays. *J. Phys. Chem. C* **2009**, *113*, 16394−16401.
(32) Bi, Y. P.; Ye, J. H. Direct Conversion of Commercial Silver Foils into High Aspect Ratio AgBr Nanowires with Enhanced Photocatalytic Properties. *Chem.—Eur. J.* **2010**, *16*, 10327−10331.